HHS Public Access

Author manuscript

Pract Radiat Oncol. Author manuscript; available in PMC 2020 November 01.

Published in final edited form as:

Pract Radiat Oncol. 2019 November ; 9(6): e534–e540. doi:10.1016/j.prro.2019.06.009.

Comparison of Motion-insensitive T2-weighted MRI Pulse Sequences for Visualization of the Prostatic Urethra during MR Simulation

Kristen L. Zakian[1,2], **Andreas Wibmer**[2], **Hebert A. Vargas**[2], **Eveline Alberts**[3], **Mo Kadbi**[3], **Borys Mychalczak**[4], **Marisa Kollmeier**[4], **Daniel Gorovets**[4], **Sean McBride**[4], **Margie Hunt**[1], **Michael J. Zelefsky**[4], **Neelam Tyagi**[1]

[1]Department of Medical Physics, Memorial Sloan Kettering Cancer Center, New York, NY [2]Department of Radiology, Memorial Sloan Kettering Cancer Center, New York, NY [3]Philips Healthcare, Best, The Netherlands [4]Department of Radiation Oncology, Memorial Sloan Kettering Cancer Center, New York, NY

Abstract

Introduction—The use of MRI for radiotherapy simulation is growing due to its ability to provide excellent delineation of target tissue and organs at risk. With the use of hypofractionated schemes in prostate cancer, urethral sparing is essential; however, visualization of the prostatic urethra can be challenging due to the presence of benign prostatic hyperplasia as well as respiratory motion artifacts. The goal of this study was to compare the utility of two motion-insensitive, T2-weighted MRI pulse sequences for urethra visualization in the setting of MRI-based simulation.

Methods—Twenty-two patients undergoing MRI simulation without Foley catheter were imaged on a 3 Tesla MR Scanner from October 2018 to January 2019. Sagittal multislice data were acquired using 1) radial sampling with parallel imaging acceleration (MVXD) and 2) single-shot fast-spin-echo (SSFSE) sequences with acquisition times of 2-3 minutes per sequence. For each exam, two genitourinary radiologists scored prostatic urethra visibility on a 1-5 scale and rated the signal-to-noise ratio and the presence of artifacts in each series.

Results—Urethral visibility was scored higher in the MVXD series than in the SSFSE series in 18 of 22 cases (Reader 1) and 17 of 22 cases (Reader 2). The differences in scores between MVXD and SSFSE were statistically significant for both readers ($P < 0.0001$ for both, paired student T test) and inter-observer agreement was high (kappa = 0.67). Both readers found the SNR of the MVXD sequence to be superior in all cases. The MVXD sequence was found to generate

Corresponding Author: Kristen L. Zakian, Ph.D., Department of Medical Physics, Memorial Sloan Kettering Cancer Center, 1275 York Avenue, New York, NY 10065, (646) 888 3465, zakiank@mskcc.org.

This work was presented at the International Society for Magnetic Resonance in Medicine 27th Annual Meeting, Montreal, CA, May 2019.

more artifacts than the SSFSE sequence, but these tended to appear in the periphery and did not affect the ability to visualize the urethra.

Conclusion—A radial T2 weighted multislice pulse sequence was superior to a single-shot fast-spin echo sequence for visualization of the urethra in the setting of MR Simulation for prostate cancer.

Introduction

The use of MRI for radiation therapy simulation is gaining in popularity due to the excellent soft-tissue delineation possible with the technique. Improved anatomic visualization of the prostatic base and apex as well as the dominant intra-prostatic lesions increases the potential for achieving higher tumor doses while maintaining normal-tissue sparing. Urethral sparing, as demonstrated in Figure 1, is essential in order to avoid significant toxicity, in particular for modern fractionation schemes (e.g. stereotactic body radiation therapy (SBRT) or external beam boost following a brachytherapy implant) [1]. Unfortunately, visualization of the entire course of the prostatic urethra on MRI can be challenging. While portions of the prostatic urethra are typically visible on T2-weighted imaging, the tortuosity and frequent compression of the urethra in the presence of benign prostatic hyperplasia (BPH) can make visualization of its entire length difficult. This difficulty can be further compounded by the presence of artifacts due to lower abdominal respiratory motion as well as peristalsis. Conventional T2-weighted pulse sequences used for prostate imaging and simulation in our department have included small field-of-view axial T2 fast-spin-echo, and sagittal multislice fast spin echo or 3D balanced fast gradient echo. In the axial sequence, the urethra in the proximal prostate gland was difficult to discern, particularly due to BPH, while the two sagittal sequences tended to suffer from motion artifact, and the radiologists and radiation oncologists at our institution concurred that these images could not be used reliably to identify the prostatic urethra. For accurate depiction of the urethra in patients undergoing simulation for SBRT, some centers employ a Foley catheter; however, this greatly increases patient discomfort and may result in altered position of the urethra compared to treatment as a Foley catheter is not employed during external beam irradiation. Therefore, we are investigating image optimization for visualization of the prostatic urethra without a Foley catheter.

The goal of the current study was to compare two clinically-available, FDA-approved T2-weighted MRI pulse sequences which are less prone to motion artifacts and blurring than standard Cartesian fast-spin-echo sequences. The two sequences evaluated were 1) Multivane XD (MVXD) (Philips Healthcare, Best, The Netherlands) which is a 2D multislice radial fast-spin-echo sequence based on PROPELLER [2] where Cartesian phase encoding with SENSE [3] parallel imaging acceleration is incorporated within each blade, and 2) Cartesian single-shot fast-spin echo (SSFSE) with SENSE acceleration. Images in the sagittal orientation were obtained with these two sequences in 22 prostate cancer patients to determine whether one technique is superior for visualization of the prostatic urethra.

Methods and Materials

Twenty-two patients undergoing MRI-based simulation for moderately hypofractionated or standard fractionation treatment were imaged from October 1, 2018 to January 14, 2019. These patients did not undergo Foley catheter placement. All MRI exams were performed on a 3 Tesla Philips Ingenia MR Scanner (Philips Healthcare, Best, The Netherlands) using the vendor's combined 32-channel anterior and 12-channel posterior receiver arrays. Conventional imaging series included large field-of-view (FOV) Dixon-based [4] T1-weighted dual-gradient-echo, small FOV axial T2 fast-spin-echo, and sagittal multislice fast spin echo or 3D balanced fast gradient echo (bFFE). Because patients were scanned with a full bladder, exam time was limited. Therefore, the MVXD and SSFSE sequences were optimized to provide sub-millimeter in-plane resolution, thin slices and adequate SNR for urethral visualization in a 2-3 minute scan time. Parameters common to both sequences were: FOV = 220-300 mm^2, in-plane resolution = 0.9×0.9, slice thickness = 2.5 mm, TR = 3500 ms, TE_{eff} = 80 ms. MVXD-specific parameters included: echoes per shot/blade = 35, averages = 1, percent of cartesian sampling = 220, SENSE acceleration = 1.8, and no partial-Fourier sampling. SSFSE-specific parameters included echo train length 79-96, SENSE acceleration = 2.0, and partial Fourier sampling percentage = 60%. Preliminary experiments indicated that SNR was inadequate when SSFSE was performed using one acquisition; therefore, the SSFSE images were acquired using two-averages to provide comparable SNR to MVXD.

Two body radiologists with urologic MRI experience > 15 years and > 10 years assessed the MVXD and SSFSE images. A 1-5 scale was used to score visibility of the *prostatic* urethra where 1 = urethra not visible and 5 = urethra visible along its entire length. In addition, the readers were asked to report, based on their qualitative impressions, whether the signal-to-noise ratio was superior in one of the two series and whether artifacts were present. Pretreatment clinical information including PSA, clinical stage, biopsy Gleason score, androgen deprivation status, and presence/treatment of BPH were obtained from the medical record. PI-RADS version 2 status [5] was obtained from the MRI report.

Results

Patient demographics and pre-treatment clinical data are provided in Table 1. None of the patients had undergone prior radiation to the prostate. Sixteen of the patients had undergone at least one month of androgen deprivation therapy (ADT) and five had been previously treated invasively for BPH/obstructive symptoms. All subjects in the current study demonstrated some degree of BPH which was observable in the proximal anterior prostate gland.

The average scan time for the MVXD series was 2 min 53 s ± 22 s while the average scan time for SSFSE was 2 min 52 s ± 7 s (mean ± standard deviation). Table 2 contains the results of the reader assessments of urethra visibility in MVXD and SSFSE images. Reader 1 reported superior urethral visibility in MVXD series in 18 cases and equivalence between MVXD and SSFSE in the remaining 4 cases. Reader 2 found that MVXD gave superior urethra visibility in 17 cases, SSFSE was superior in 1 case, and the sequences were

equivalent in 4 cases. The average urethra visibility scores for the MVXD sequence were 3.7 ± 0.6 and 3.8 ± 0.9 for readers 1 and 2, respectively, while the average scores for SSFSE were 2.6 ± 0.8 and 2.8 ± 1.0 for readers 1 and 2. The differences in scores between MVXD and SSFSE were statistically significant for both readers ($P < 0.0001$ for both, paired student T test) [6]. When visibility readings were classified as MVXD superior vs MVXD not superior, inter-observer agreement was high (Cohen's kappa = 0.67) [7]. The readers' qualitative impressions of SNR and the presence of artifacts are shown in Table 3. Both readers found the SNR of the MVXD sequence to be superior in all cases. The MVXD sequence was found to generate more artifacts than the SSFSE sequence, but these streak artifacts tended to be more peripheral and in no case were found to obscure the urethra. Motion-induced blurring was not noted in either the MVXD or the SSFSE images.

Examples of T2-weighted images acquired with MVXD and SSFSE sequences are included in Figures 2 and 3. In Figure 2, anatomical structures of interest are labeled in the first frame. The bladder outlet is a useful landmark for locating the proximal prostatic urethra. In this subject, visibility of the urethra was found to be similar in MVXD and SSFSE series. Reader 1 gave a urethra visibility score of 4 for both MVXD (A-C) and SS-SSFSE (D-F) while Reader 2 scored MVXD as 3 and SS-FSE as 4. The large BPH nodule may have compressed or displaced the urethra in the prostate adjacent to the bladder. The noise levels were similar in the two series as indicated by similar levels of graininess in the prostate. Streaking artifact due to radial sampling was noted in the MVXD series but did not obscure any portion of the prostate gland. Figure 3 contains images from a patient where the readers indicated that the urethra was more visible in the MVXD images; both readers scored urethra visibility as 5 on MVXD and 3 on SSFSE.

Discussion

This study assessed the value of two fast T2-weighted MR pulse sequences for delineating the prostatic urethra as part of a rapid throughput MR Simulation workflow. Both sequences provided submillimeter in-plane resolution with 2.5 mm slice thickness in approximately 3 minutes. In our study, both expert readers determined that the SENSE-enhanced PROPELLER-based MVXD sequence performed superiorly in more than 75% of the cases. Based on the impressions of the readers, the advantage was mainly due to higher signal-to-noise ratio which reduced graininess within the prostate gland in the radial MVXD images. The source of enhanced SNR is likely the oversampling of low spatial frequencies inherent in radial techniques opposed to traditional uniformly sampled Cartesian trajectories [2].

Radial sampling reduces the appearance of motion artifacts by eliminating traditional singledirection phase encoding with its potential for inter-shot motion and ghosting; instead motion results in streak artifacts with varying orientations [8]. To obtain the same spatial resolution as a Cartesian-sampled image of equal matrix size, the number of radial spokes must be at least $\pi/2$ times the number of samples in one Cartesian dimension [2]. In our radial acquisition, we employed a 2.2 oversampling factor. Radial-sampling streak artifacts were noted in some of the MVXD images but these did not obscure the urethra. To eliminate streaking, the radial sampling factor could be further increased at the cost of a proportional

increase in scan time. However, because streak artifacts tended to be peripheral and did not interfere with visualization of the urethra, we preferred the stated oversampling factor.

Rather than altering the appearance of motion artifacts, single-shot fast-spin-echo techniques, e.g. HASTE [9] acquire images in hundreds of milliseconds, essentially capturing rapid snapshots and precluding motion artifacts. In the current study, two SSFSE images were averaged to obtain adequate signal-to-noise ratio (see Methods and Materials). Therefore, between-shot motion-induced blurring could contribute to the inferiority of the SSFSE images. However, the readers found fewer artifacts, including motion artifacts in the SSFSE images. Therefore, SNR was the main source of difference in the utility of the two sequences.

Contouring in the axial plane has been standard in treatment planning because CT images are usually acquired axially and treatment planning systems have been developed in accordance. Guidelines for contouring the urethra on T2-weighted axial pelvic MR images have been suggested by Kataria, et. al.[10]. However, MRI permits acquisition in any plane, and modern contouring systems have the capability of importing images acquired in multiple planes and permit contouring on non-axial scans. Our clinicians have found that the course of the urethra is easier to follow on sagittal images, particularly in the presence of BPH-related compression and tortuosity. In addition, the urethra in the proximal gland is angulated in the anterior-posterior dimension such that its outline loses some definition on axial sections with thickness greater than 1-2 mm. We have found no difficulty in incorporating sagittal urethra contours in our treatment planning workflow.

The high soft tissue contrast and quality of the images acquired with both types ofT2-weighted sequences indicate the potential for contouring the prostatic urethra without the use of a Foley catheter which would be beneficial to the patient in addition to simplifying the workflow. While reports of optimized urethra-specific imaging by MRI are rare, several groups have investigated MR urethrography using gadolinium-based contrast agents for the depiction of lesions and urethral strictures [11,12]. However, the effectiveness of a contrast agent for depiction of the normal urethra is not known and contrast administration would prolong the MR simulation workflow. Recognizing the necessity for urethral delineation for radiation therapy treatment planning, another group recently reported realtime MRI where patients were instructed to micturate in their own time whereupon a sagittal T2-weighted sequence was acquired every 5 seconds [13]. While this technique can be effective, this approach has some logistical drawbacks and may not be reliable. As the use of SBRT becomes more prevalent and MR-Linac systems [14,15] as well as MR Simulators are employed, direct visualization of urethra on the MR image without the use of a contrast agent, will become even more important.

One weakness of this manuscript is that quantitative measures of signal-to-noise ratio were not made. Because SENSE parallel imaging was employed, the coil combination algorithm generated spatially varying noise, and background noise was also masked by vendor reconstruction software. Therefore, accurate noise measurements were not possible, and we reported qualitative SNR assessments. The good agreement between the expert readers suggests that the SNR superiority in the MVXD images was not spurious.

Conclusion

A radial, PROPELLER-based, SENSE-enhanced T2 weighted pulse sequence was superior to a single-shot fast-spin echo sequence for visualization of the prostatic urethra. High contrast and spatial resolution within a rapid scan time make this sequence practical in the clinic, potentially sparing patients the discomfort of Foley catheter insertion while allowing accurate urethral delineation and dose-sparing in the treatment planning process. Future work will explore the integration of MR-based urethra delineation with our existing clinical treatment planning workflow.

Acknowledgments

Disclosures:

Memorial Sloan Kettering Cancer Center and Philips Healthcare have a Research Collaboration Agreement

Dr. Wibmer has been supported by the Peter Michael Foundation

This research was partially supported by the NIH/NCI Cancer Center Support Grant/Core Grant (P30 CA008748).

References

[1]. Repka MC, Guleria S, Cyr RAet al. Acute Urinary Morbidity Following Stereotactic Body Radiation Therapy for Prostate Cancer with Prophylactic Alpha-Adrenergic Antagonist and Urethral Dose Reduction. Frontiers in oncology 2016;6:122. [PubMed: 27242962]

[2]. Pipe JG. Motion correction with PROPELLER MRI: application to head motion and free-breathing cardiac imaging. Magn Reson Med 1999;42(5):963–969. [PubMed: 10542356]

[3]. Pruessmann KP, Weiger M, Scheidegger MB, Boesiger P. SENSE: sensitivity encoding for fast MRI. Magn Reson Med 1999;42(5):952–962. [PubMed: 10542355]

[4]. Dixon WT. Simple proton spectroscopic imaging. Radiology 1984;153(1):189–194. [PubMed: 6089263]

[5]. Prostate Imaging Reporting and Data System. American College of Radiology (ACR) 2015 https://www.acr.org/Clinical-Resources/Reporting-and-Data-Systems/PI-RADS.

[6]. Rice JA. Mathematical Statistics and Data Analysis: Duxbury; 2007.

[7]. Cohen J A Coefficient of Agreement for Nominal Scales. Educational and Psychological Measurement 1960;20(1):37–46.

[8]. Glover GH, Pauly JM. Projection reconstruction techniques for reduction of motion effects in MRI. Magn Reson Med 1992;28(2):275–289. [PubMed: 1461126]

[9]. Patel MR, Klufas RA, Alberico RA, Edelman RR. Half-fourier acquisition single-shot turbo spin-echo (HASTE) MR: comparison with fast spin-echo MR in diseases of the brain. AJNR Am J Neuroradiol 1997;18(9):1635–1640. [PubMed: 9367310]

[10]. Kataria T, Gupta D, Goyal S et al. Simple diagrammatic method to delineate male urethra in prostate cancer radiotherapy: an MRI based approach. Br J Radiol 2016;89(1068):20160348. [PubMed: 27748126]

[11]. Hanna S AZ, Abdel Rahman S F, Altamimi BA, Shoman AM. Role of MR Urethrography in Assessment of Urethral Lesions. The Egyptian Journal of Radiology and Nuclear Medicine 2015;46(2):499–505.

[12]. Osman Y, El-Ghar MA, Mansour O, Refaie H, El-Diasty T. Magnetic resonance urethrography in comparison to retrograde urethrography in diagnosis of male urethral strictures: is it clinically relevant? Eur Urol 2006;50(3):587–593; discussion 594. [PubMed: 16457942]

[13]. Rai R, Sidhom M, Lim K, Ohanessian L, Liney GP. MRI micturating urethrography for improved urethral delineation in prostate radiotherapy planning: a case study. Phys Med Biol 2017;62(8):3003–3010. [PubMed: 28306557]

[14]. Wen N, Kim J, Doemer A et al. Evaluation of a magnetic resonance guided linear accelerator for stereotactic radiosurgery treatment. Radiother Oncol 2018;127(3):460–466. [PubMed: 29807837]

[15]. Menten MJ, Fast MF, Nill Set. et al. Lung stereotactic body radiotherapy with an MR-linac - Quantifying the impact of the magnetic field and real-time tumor tracking. Radiother Oncol 2016;119(3):461–466. [PubMed: 27165615]

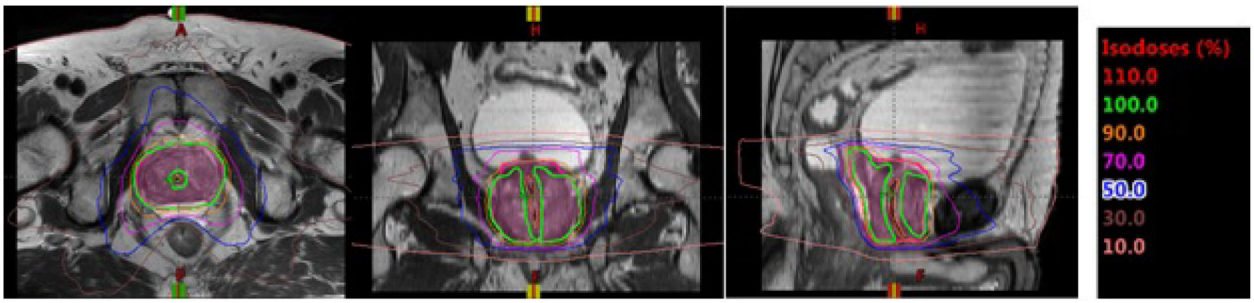

Figure 1:
Isodose line displayed on a T2-weighted MR image for a patient planned for five-fraction stereotactic body radiation therapy (SBRT). Dose around the urethra was reduced to meet institutional guidelines for urethra.

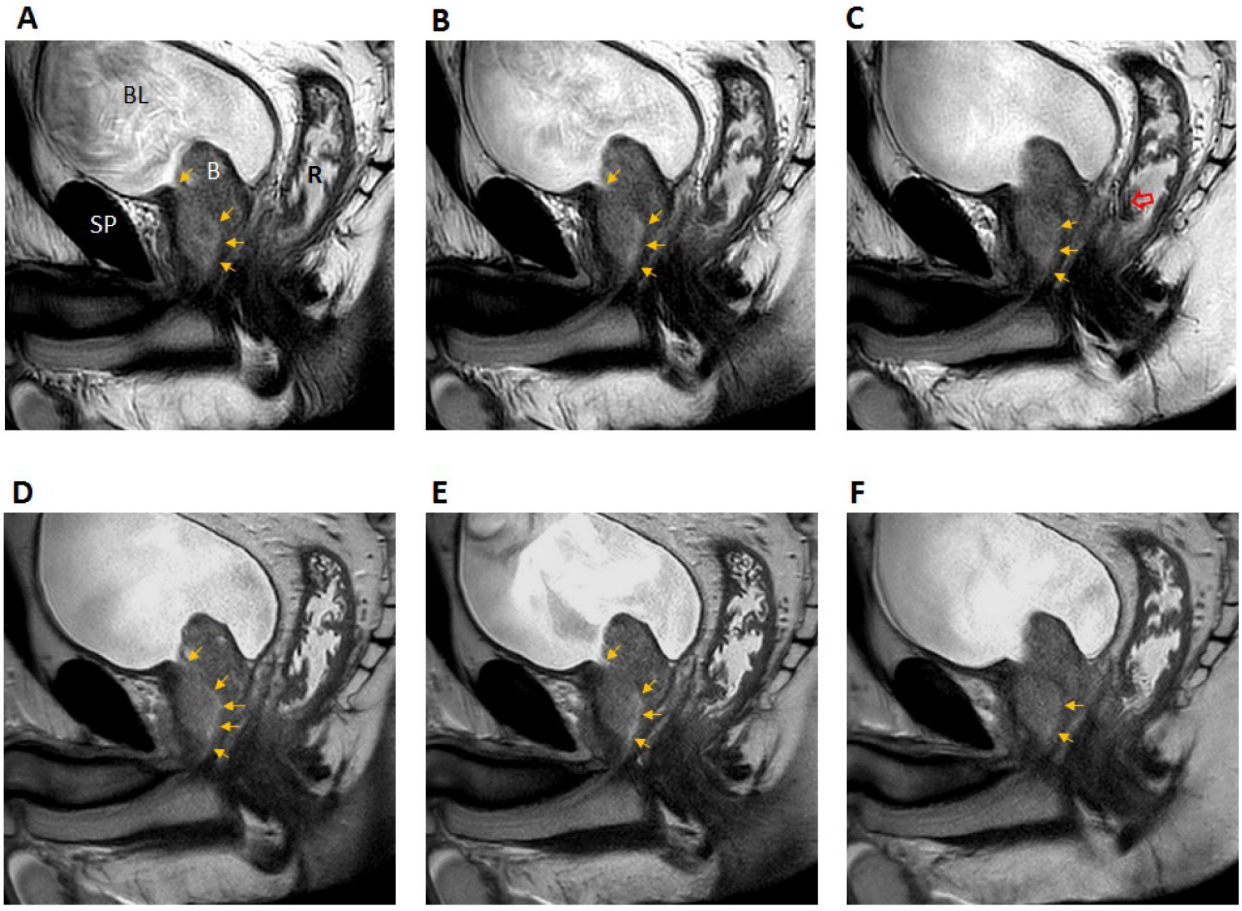

Figure 2.

Consecutive T2-weighted sagittal sections through the prostatic urethra (top row MVXD, bottom row SSFSE). In frame A, the following structures are labeled: BL = bladder; SP = symphysis pubis; R = rectal cavity, B = large BPH nodule. The prostatic urethra is indicated by gold arrows. The open red arrow indicates radial streaking artifact. Grayscale window and level were adjusted for maximum visibility of the urethra. Scan times were 2 min 35 s for MVXD and 2 min 30 s for SSTSE. See text for all scan parameters. Reader scores for urethral visibility in MVXD vs SSFSE were 4 vs. 4 (Reader 1) and 3 vs. 4 (Reader 2).

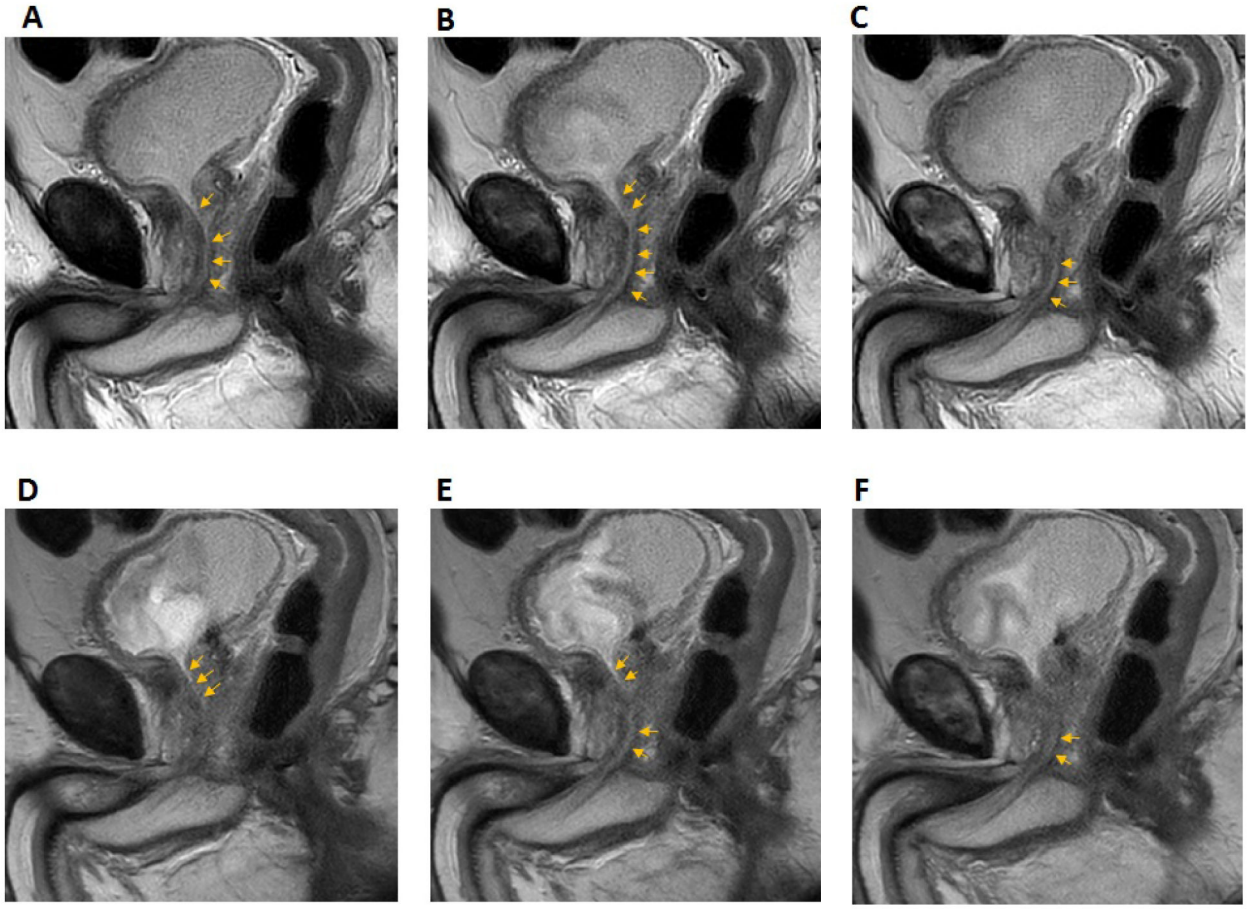

Figure 3.

Consecutive T2-weighted sagittal sections through the prostatic urethra (MVXD top row, SSFSE bottom row). See text for scan parameters. Scan times were 2 min 37 s for MVXD and 2 min 55 s for SSTSE. Reader scores for urethral visibility in MVSD vs SSFSE were 5 vs. 3 (Reader 1) and 5 vs. 3 (Reader 2).

Table 1.

Pre-Treatment Clinical Data for Study Population. “u” indicates data unavailable.

Subject	PSA	Gleason Score	Age	Stage	PI-RADS Score*	ADT	Prior TURP/BPH Reduction
1	4.2	3+4	68	T1c	4	n	n
2	6.1	4+3	69	T1c	4	y	y
3	5.48	4+3	79	T2b	5	n	n
4	7.1	4+5	78	T1c	4	y	n
5	8.1	3+4	68	T3a	5	y	n
6	12.28	4+5	74	T3a	5	y	n
7	676	4+4	42	T4	5	y	n
8	18.4	4+3	80	T3a	5	y	n
9	30.7	5+5	56	T3b	5	y	n
10	1.3	4+3	76	T2c	5	n	y
11	6.39	3+4	71	T1c	5	n	y
12	6.1	3+4	73	T1c	5	n	n
13	27.64	3+4	74	T1c	5	y	n
14	8	4+4	84	u	5	y	n
15	6.26	4+3	74	T1c	3	y	n
16	11	3+4	59	T1c	4	y	n
17	23.36	5+4	59	T3b	5	y	n
18	19	4+3	69	T3a	5	y	n
19	9.62	u	81	u	5	y	n
20	4.81	4+3	77	T2b	4	y	y
21	5	3+4	79	T1c	5	n	y
22	44.9	5+4	82	T4	5	y	n

*While all patients were assigned PI-RADS scores as part of an ongoing study, the PI-RADS score is defined only in the pre-treatment setting.

Table 2.

Urethra visibility results. A 1-5 scale was used to score visibility of the prostatic urethra where 1 = urethra not visible and 5 = urethra visible along its entire length.

	Urethra Visibility Score (Reader 1)		Urethra Visibility Score (Reader 2)	
Subject	**MVXD**	**SSFSE**	**MVXD**	**SSFSE**
1	4	4	3	4
2	4	3	4	3
3	4	4	4	4
4	4	2	4	2
5	3	2	3	2
6	4	3	4	3
7	4	2	4	2
8	4	3	4	2
9	3	2	4	2
10	4	2	5	3
11	4	3	5	4
12	4	4	5	5
13	3	2	3	2
14	3	1	3	2
15	3	1	4	3
16	3	2	2	1
17	4	3	4	4
18	3	3	2	2
19	4	3	5	4
20	5	3	5	3
21	4	3	3	2
22	4	3	4	3
Mean ± standard deviation	3.7 ± 0.6	2.6 ± 0.8	3.8 ± 0.9	2.8 ± 1.0

Table 3.

Signal-to-noise ratio and artifact results. MV = MVXD, SS = SSFSE, B both pulse sequences, N = neither pulse sequence.

	Reader 1		Reader 2	
Subject	**Superior SNR**	**Artifact Present**	**Superior SNR**	**Artifact Present**
1	MV	MV	MV	B
2	MV	MV	MV	MV
3	MV	MV	MV	MV
4	MV	MV	MV	MV
5	MV	N	MV	N
6	MV	N	MV	N
7	MV	MV	MV	N
8	MV	N	MV	N
9	MV	N	MV	N
10	MV	N	MV	N
11	MV	N	MV	N
12	MV	N	MV	N
13	MV	N	MV	N
14	MV	N	MV	N
15	MV	N	MV	MV
16	MV	N	MV	N
17	MV	N	MV	N
18	MV	N	MV	MV
19	MV	N	MV	N
20	MV	N	MV	N
21	MV	N	MV	N
22	MV	SS	MV	N